applied optics

Measurement method of high spectral resolution lidar with a multimode laser and a scanning Mach–Zehnder interferometer

Yoshitaka Jin,[1,*] Nobuo Sugimoto,[1] Pablo Ristori,[2] Tomoaki Nishizawa,[1] Lidia Otero,[2] and Eduardo Quel[2]

[1]Center for Environmental Measurement and Analysis, National Institute for Environmental Studies, 16-2 Onogawa, Tsukuba, Ibaraki 305-8506, Japan
[2]CEILAP, UNIDEF (MINDEF–CONICET), Juan Bautista de La Salle 4397, B1603ALO, Villa Martelli, Provincia de Buenos Aires, Argentina
*Corresponding author: jin.yoshitaka@nies.go.jp

Received 9 May 2017; revised 24 June 2017; accepted 24 June 2017; posted 26 June 2017 (Doc. ID 295467); published 19 July 2017

A simple high spectral resolution lidar technique using a multi-longitudinal mode laser is proposed for measuring aerosol extinction and backscattering coefficients. A scanning interferometer having the same free spectral range as the mode spacing of the laser is used to separate Rayleigh from Mie scattering. Scanning the interferometer in the span of one fringe, the lidar signals at the minimum and maximum Mie-scattering transmission are measured. The Rayleigh scattering signal is analyzed from these signals, and the aerosol extinction coefficient is derived. The interferometer transmittance for Mie scattering is calibrated with the reference signals taken with a portion of the transmitted laser beam.

OCIS codes: (010.3640) Lidar; (120.3180) Interferometry; (010.1110) Aerosols; (290.2200) Extinction; (290.1350) Backscattering.

https://doi.org/10.1364/AO.56.005990

1. INTRODUCTION

Continuous observation of aerosol distribution and optical characteristics is indispensable for understanding the effects of aerosols on the environment and climate. Widely used elastic lidars are useful for measuring aerosol profiles. However, the assumption of the extinction-to-backscattering ratio (lidar ratio) required in the retrieval of the extinction coefficient can cause a problem in the quantitative data use. Raman lidar and high spectral resolution lidar (HSRL) use methods for measuring the aerosol extinction coefficient independently from the aerosol backscattering coefficient.

HSRL utilizes the attenuation of the atmospheric molecular Rayleigh scattering to measure the aerosol extinction coefficient. Since vertical distribution of atmospheric molecules is known from radiosonde observations or reanalysis data, the aerosol extinction coefficient can be retrieved from the measured Rayleigh scattering signals by solving the lidar equation. A high spectral resolution optical element, such as an etalon or a molecular filter, is usually employed to separate the Mie scattering by aerosols from the Doppler-broadened Rayleigh scattering by atmospheric molecules. Aerosol extinction can also be measured with Raman lidars. However, the scattering cross-section of nitrogen vibrational Raman scattering at 607 nm is three orders of magnitude smaller than that of the Rayleigh scattering at 532 nm, and consequently daytime measurement of aerosol extinction with Raman lidars is difficult.

Measurement of Mie and Rayleigh scattering spectra was first demonstrated using a scanning Fabry–Perot interferometer to obtain air temperature [1]. Aerosol extinction and backscattering coefficients were first measured by separating Mie and Rayleigh scattering components using a high spectral resolution etalon [2]. Methods using atomic filters [3] and molecular filters [4,5] have also been developed to separate Mie and Rayleigh scattering signals. Recently, airborne HSRLs were developed [6–8], and a spaceborne HSRL (ATLID/EarthCARE) is planned for launch [9].

HSRL will be a key player also in continuous ground-based lidar network observations. Independent measurement of extinction and backscatter also improves aerosol type classification [10] and the retrieval of aerosol components [11]. However, traditional HSRLs require high-cost, single-longitudinal-mode lasers and a complicated control of the laser and/or the spectrometer. That makes widespread use of HSRLs difficult. Continuous observations using HSRLs are reported [12], but it is not common so far, probably for the above reasons. Low-cost, simple HSRLs are necessary for expanding the use of HSRLs.

This study describes a new concept of multimode HSRL (MM-HSRL) using a multi-longitudinal, single-transverse mode laser that is widely used for aerosol lidars. A scanning

Mach–Zehnder interferometer with the same mode spacing as the multimode laser is used in the receiver as a high-resolution spectral element. A direct-detection Doppler lidar with a multimode laser and a Mach–Zehnder interferometer is previously reported [13], but the concept is different. In this study, the scanning Mach–Zehnder interferometer is used as a rejection filter. If the transmittance minima of the interferometer are matched to the longitudinal modes of the laser, the Mie scattering component can be removed, and the Doppler-broadened Rayleigh scattering component is measured. The interferometer is periodically scanned in the span of one fringe to analyze the minimum (maximum) of interferometer transmittance. Therefore, the system does not require any feedback for laser wavelength control. The target of our study is to develop a durable MM-HSRL for long-term aerosol extinction measurement in daytime and nighttime with a higher sensitivity than nighttime Raman lidars.

In this paper, we describe the lidar system, the data analysis method to retrieve aerosol extinction and backscattering coefficients, and the error analysis. We also show measurements of atmospheric aerosols using the technique.

2. SYSTEM USING A MACH–ZEHNDER INTERFEROMETER

The lidar system employs a multimode Nd:YAG laser (Continuum Surelite I) with a second harmonic generation (Fig. 1). Linewidth of the laser is 1 cm^{-1}. The repetition rate of the laser is 10 Hz. Beam divergence is 0.1 mrad (full angle) after a 5-time beam expander. The pulse energy of the laser is 200 mJ at 532 nm.

In the receiver part, an 8-inch telescope (Celestron C8) is employed. A Mach–Zehnder interferometer with two half mirrors and a roof mirror mounted on a piezo stage is used as a high-spectral-resolution optical element. A portion of the transmitted laser light is directed to the receiver telescope and used as a reference signal to evaluate the transmittance of the interferometer for the laser spectrum (the Mie scattering component). The interferometer length (distance from the half mirrors to the roof mirror) is adjusted to the length where the free spectral range (FSR) of the interferometer is the same as the laser mode spacing. The proper length is determined by maximizing the interferometer contrast for the reference light. The determined interferometer length is 59 cm, which corresponds to the laser mode spacing of 255 MHz. The experiment for determining the interferometer length is described in Section 3.C.

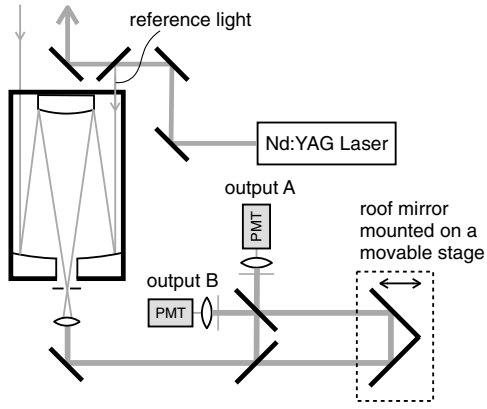

Fig. 1. Block diagram of a HSRL with a multimode laser and a Mach–Zehnder interferometer.

For the lidar measurement, the interferometer is periodically scanned with a scanning range equal to the laser mode spacing. The roof mirror is scanned half of the laser wavelength using the piezo stage driven by a function generator. In this study, scanning speed is set to 1 Hz (i.e., 10 shots per sweep). The lidar signals are detected with two photomultiplier tubes at the two arms of the interferometer (A and B in Fig. 1) and recorded shot per shot at 100 mega samples per second (i.e., 1.5-m height resolution).

Lidar signal profiles from the system consist of the reference signals and the atmospheric scattering signals (Fig. 2). The signal strength changes depending on the relative position of the laser mode frequencies and the interferometer spectrum. When the transmittance minima match the peaks of the laser spectrum, the Mie scattering component is rejected most efficiently, resulting in the lowest signal strength, and it mostly consists of Doppler-broadened Rayleigh scattering (blue line in Fig. 2). However, even at the minimum Mie transmittance position, part of the Mie component remains as a bias (cross-talk) due to the laser spectral width. This bias component must be removed from the signals to obtain Rayleigh signals for retrieving the aerosol extinction coefficient. The reference signal is used for this purpose.

Part of the Rayleigh scattering component is also rejected by the interferometer, but it is not dependent on the relative position of the interferometer spectrum if the FSR of the interferometer is sufficiently smaller than the spectral width of Rayleigh scattering. The spectral width of Rayleigh scattering is a few GHz, depending on the temperature, and the FSR of the interferometer (the same as the laser mode spacing) is much smaller. The transmittance for Rayleigh scattering consequently can be assumed to be 0.5.

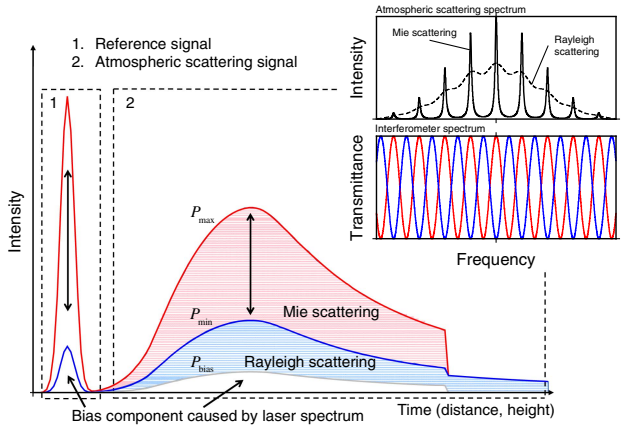

Fig. 2. Schematic diagram of the lidar signals from the system. Atmospheric scattering and interferometer transmittance spectra are also shown. Minimum (maximum) signals are obtained when minima (maxima) of interferometer transmittance match the longitudinal modes of the laser as denoted by the blue (red) lines. The gray line denotes the intensity of the bias component contained in the minimum signals. The two-way arrows denote the intensity variation with the interferometer scan (See Visualization 1).

3. ANALYSIS METHOD

This section describes a procedure for retrieving aerosol backscattering and extinction coefficients from the MM-HSRL signals. A fitting method for scanned data is also described.

A. Retrieval of Backscattering and Extinction Coefficients

Lidar signals for output A (P_A) in Fig. 1 are described as

$$P_A(r) = \frac{K_A}{r^2} Y(r)[X_1\beta_1(r) + X_2\beta_2(r)]T^2. \quad (1)$$

Here, r is the range (or height), K is the calibration constant, Y is the overlap function (or geometrical form factor), β is the backscattering coefficient, T^2 is the two-way atmospheric transmittance from the lidar to r, and X is the interferometer transmittance for atmospheric scattering light. Subscript 1 denotes the particle (or Mie scattering) component, and subscript 2 denotes the molecular (or Rayleigh scattering) component. Signals of the opposite phase (ouput B, P_B) are expressed by replacing X_1 as $(1 - X_1)$ and X_2 as $(1 - X_2)$. Relative sensitivity between P_A and P_B is calibrated beforehand, and hence hereafter we use the calibration constant K without subscripts.

Here we define the minimum (maximum) X_1 as $X_1^{\min}$ ($X_1^{\max}$) where the minima (maxima) of the interferometer transmittance match the longitudinal modes of the laser. When X_1 is $X_1^{\min}$ ($X_1^{\max}$), the Mie scattering signals' strength is the smallest (largest). The smallest lidar signals ($P_{\min}$) are expressed as

$$P_{\min}(r) = \frac{K}{r^2} Y(r)[X_1^{\min}\beta_1(r) + 0.5\beta_2(r)]T^2, \quad (2)$$

where X_2 is assumed to 0.5, as discussed earlier. $P_{\max}$ is expressed by replacing $X_1^{\min}$ as $X_1^{\max}$ in Eq. (2). Because $X_1^{\min} + X_1^{\max}$ is 1, $P_{\min} + P_{\max}$ is expressed as

$$P_{\min}(r) + P_{\max}(r) = \frac{K}{r^2} Y(r)[\beta_1(r) + \beta_2(r)]T^2. \quad (3)$$

$P_{\min}$ and $P_{\max}$ are estimated from the periodically scanned P_A and P_B signals. The method for the estimation is described in the next subsection. Higher contrast between $P_{\min}$ and $P_{\max}$ is obtained when the contribution of Mie scattering is higher.

With Eqs. (2) and (3), the aerosol backscattering coefficient is derived by the following equation:

$$\beta_1(r) = \beta_2(r)\left[\frac{0.5 - P_{\text{rat}}^{\min}(r)}{P_{\text{rat}}^{\min}(r) - X_1^{\min}}\right], \quad (4)$$

where $P_{\text{rat}}^{\min}$ is the interference contrast given as

$$P_{\text{rat}}^{\min}(r) = \frac{P_{\min}(r)}{P_{\min}(r) + P_{\max}(r)}. \quad (5)$$

$P_{\text{rat}}^{\min}$ approaches $X_1^{\min}$ as the total-to-molecular backscattering ratio increases, and $P_{\text{rat}}^{\min}$ reaches 0.5 when the total-to-molecular backscattering ratio is 1. In Eq. (4), the backscattering coefficient is normalized by the Rayleigh scattering and is independent of the calibration constant and the atmospheric transmittance.

The aerosol extinction coefficient α_1 is calculated from the gradient of the Rayleigh scattering signals by the following equation:

$$\alpha_1(r) = \frac{1}{2\Delta r}\ln\left[\frac{P_{\text{Ray}}(r-\Delta r/2)(r-\Delta r/2)^2/\beta_2(r-\Delta r/2)}{P_{\text{Ray}}(r+\Delta r/2)(r+\Delta r/2)^2/\beta_2(r+\Delta r/2)}\right]_{-\alpha_2(r)}, \quad (6)$$

where Δr is a range interval for calculating the gradient and is set to 300 m in this study. The molecular backscattering (β_2) and extinction (α_2) are calculated from radiosonde data or modeled data, or the standard atmosphere. Rayleigh scattering signals P_{Ray} can be derived by subtracting the bias component P_{bias} from $P_{\min}$ as follows:

$$P_{\text{Ray}}(r) = \frac{K}{2r^2} Y(r)\beta_2(r)T^2 = P_{\min}(r) - P_{\text{bias}}(r), \quad (7)$$

where

$$P_{\text{bias}}(r) = \frac{X_1^{\min}[P_{\max}(r) - P_{\min}(r)]}{1 - 2X_1^{\min}}. \quad (8)$$

P_{bias} can change depending on the Mie scattering intensity as shown in Fig. 2.

B. Fitting Method for the Scanned Lidar Data

As described in the preceding section, parameters $X_1^{\min}$, $P_{\min}$, and $P_{\max}$ are required to derive the backscattering and the extinction coefficients. $P_{\min}$ is derived from the following equation:

$$P_{\min}(r) = P_{\text{rat}}^{\min}(r)\frac{1}{N}\sum_{t=1}^{N}[P_A(r,t) + P_B(r,t)], \quad (9)$$

where N is the number of profiles. $P_{\max}$ is derived by replacing $P_{\text{rat}}^{\min}$ as $P_{\text{rat}}^{\max}$. Therefore $P_{\text{rat}}^{\min}$ ($P_{\text{rat}}^{\max}$) is needed to derive $P_{\min}$ ($P_{\max}$). The method for estimating $X_1^{\min}$ and $P_{\text{rat}}^{\min}$ is the same. $X_1^{\min}$ is estimated from the reference signals, and $P_{\text{rat}}^{\min}$ is estimated from the atmospheric scattering signals.

X_1 is the ratio of the reference signal (output A or B) to the total reference signal (output $A + B$). Here, we assume the laser (reference light) spectrum is the same as the Mie scattering spectrum. X_1 is expressed as

$$X_1 = \frac{P_A^{\text{Ref}}}{P_A^{\text{Ref}} + P_B^{\text{Ref}}}, \quad (10)$$

where the superscript Ref denotes reference signals. $X_1^{\min}$ is estimated by fitting a modeled cosine curve to the periodically scanned X_1 data. The model curve is given by

$$X_1^{\text{mod}}(\theta) = 0.5 + C_1\cos(\theta + C_2), \quad (11)$$

where C_1 and C_2 are parameters of amplitude and phase, respectively. The curve fitting is applied every scan (10 shots) with a non-linear least square method. The phase parameter C_2 changes are associated with the shift of the laser spectrum. Using the estimated C_2, the phase of X_1 is corrected every scan. The curve fitting is finally applied to all the phase-corrected X_1 data during the observation time. $X_1^{\min}$ is then taken from the minimum value of X_1^{mod} (i.e., $|\theta| = \pi$).

P_{rat} is derived by calculating the ratio of an atmospheric scattering signal (output A or B) to the total signal (output $A + B$). The same C_2 determined for X_1 is used for P_{rat} every scan. The phase corrected P_{rat} is then approximated by the modeled

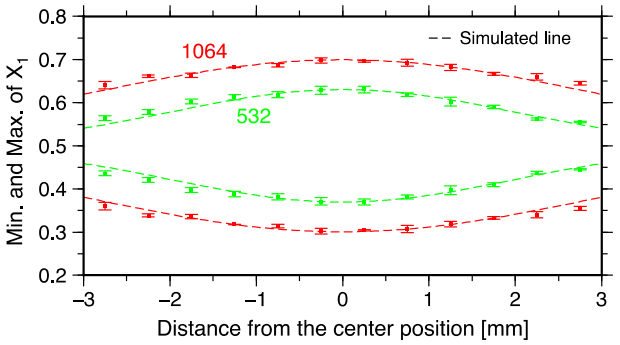

Fig. 3. Minimum and maximum of interferometer transmittance for the laser (X_1) as a function of the interferometer length. The center of the x axis corresponds to the interferometer length where the FSR of the interferometer is matched to the laser mode spacing. The error bars denote the standard deviation of the measured values.

curve of Eq. (11) but for $P_{\mathrm{rat}}^{\mathrm{mod}}$ instead of X_1^{mod}, using all data in the observation time. $P_{\mathrm{rat}}^{\mathrm{min}}$ ($P_{\mathrm{rat}}^{\mathrm{max}}$) is taken from the minimum (maximum) of $P_{\mathrm{rat}}^{\mathrm{mod}}$.

C. Measurement of X_1^{min} with the Reference Signals

We measured X_1 using the reference signals, changing the interferometer length step by step. Figure 3 shows the minimum and maximum of X_1 as a function of interferometer length. The strongest contrast of interference was observed at the position where the FSR of the interferometer matched the laser mode spacing. The interferometer length for the strongest contrast was 59 cm, and the FSR was 255 MHz.

Measured values of X_1^{min} (X_1^{max}) were 0.3 (0.7) and 0.37 (0.63) at 1064 nm and 532 nm, respectively. Nominal mode spacing at 532 nm is the same as that at 1064 nm, because of the sum frequency generation caused by the multimode at 1064 nm. Using the measured X_1^{min} and X_1^{max}, the spectral width of each mode can be estimated based on a simulation study [14]. The estimated spectral width is 77 MHz at 1064 nm, and the corresponding reflectivity of the front mirror of the cavity is 17%. This value agrees with the technical data of the Continuum Surelite I. Also, the estimated spectral width at 532 nm is 116 MHz, and the factor 1.5 compared to 1064 nm is consistent with the data sheet of the linewidth at 532 nm for Surelite I. Consequently, the simulated lines are in good agreement with the experimental results (Fig. 3).

4. ERROR ANALYSIS

The backscattering coefficient can be retrieved using $P_{\mathrm{rat}}^{\mathrm{min}}$ and X_1^{min} as described in Eq. (4). Random and systematic errors in the retrieved backscattering coefficient are expressed as

$$\left(\frac{\delta\beta_1(r)}{\beta_1(r)}\right)_{\mathrm{ram}} = \frac{R^2(r)\Delta P_{\mathrm{rat}}^{\mathrm{min}}(r)}{(0.5 - X_1^{\mathrm{min}})(R(r) - 1)}, \tag{12}$$

$$\left(\frac{\delta\beta_1(r)}{\beta_1(r)}\right)_{\mathrm{sys}} = \frac{R(r)\Delta X_1^{\mathrm{min}}}{(0.5 - X_1^{\mathrm{min}})} + \frac{\Delta\beta_2}{\beta_2}, \tag{13}$$

where R is the total-to-molecular backscattering ratio (i.e., $R = (\beta_1 + \beta_2)/\beta_2$), and subscripts ram and sys denote random and systematic, respectively. $\Delta X_1^{\mathrm{min}}$ can be ignored for random errors because the signal-to-noise ratio of the reference signals is much higher than that of the atmospheric scattering signals. If R is 2.0, required $\Delta P_{\mathrm{rat}}^{\mathrm{min}}/P_{\mathrm{rat}}^{\mathrm{min}}$ is 0.75% to obtain less than 10% errors in the retrieved backscattering. This means that the needed signal-to-noise ratio is approximately 100. For the systematic error, required $\Delta X_1^{\mathrm{min}}/X_1^{\mathrm{min}}$ is approximately 2% to obtain less than 10% errors. Uncertainty of temperature profiles causes errors in the calculation of molecular backscattering, if the standard atmosphere is used. The error is usually negligibly small and appears only for the case of strong inversion layers.

Random and systematic errors in the retrieved aerosol extinction coefficient are expressed as

$$\left(\frac{\delta\alpha_1(r)}{\alpha_1(r)}\right)_{\mathrm{ram}} = \frac{1}{2\alpha_1(r)\Delta r}\left\{\left[\left(\frac{\delta P_{\mathrm{Ray}}(r - \Delta r/2)}{P_{\mathrm{Ray}}(r - \Delta r/2)}\right)_{\mathrm{ram}}\right]^2 + \left[\left(\frac{\delta P_{\mathrm{Ray}}(r + \Delta r/2)}{P_{\mathrm{Ray}}(r + \Delta r/2)}\right)_{\mathrm{ram}}\right]^2 + [2(\delta\alpha_2(r))_{\mathrm{ram}}\Delta r]^2\right\}^{1/2}, \tag{14}$$

$$\left(\frac{\delta\alpha_1(r)}{\alpha_1(r)}\right)_{\mathrm{sys}} = \frac{1}{2\alpha_1(r)\Delta r}\left\{\left(\frac{\delta P_{\mathrm{Ray}}(r - \Delta r/2)}{P_{\mathrm{Ray}}(r - \Delta r/2)}\right)_{\mathrm{sys}} - \left(\frac{\delta P_{\mathrm{Ray}}(r + \Delta r/2)}{P_{\mathrm{Ray}}(r + \Delta r/2)}\right)_{\mathrm{sys}} - 2(\delta\alpha_2(r))_{\mathrm{sys}}\Delta r\right\}. \tag{15}$$

Random errors in estimated P_{Ray} are given as

$$\left(\frac{\delta P_{\mathrm{Ray}}(r)}{P_{\mathrm{Ray}}(r)}\right)_{\mathrm{ram}} = \frac{X_1^{\mathrm{min}}(1 - X_1^{\mathrm{min}})}{1 - 2X_1^{\mathrm{min}}}\left\{\left[\left(\frac{1}{X_1^{\mathrm{min}}} + \frac{2\beta_1(r)}{\beta_2(r)}\right)\frac{1}{\mathrm{SNR}_{\mathrm{min}}}\right]^2 + \left[\left(\frac{1}{1 - X_1^{\mathrm{min}}} + \frac{2\beta_1(r)}{\beta_2(r)}\right)\frac{1}{\mathrm{SNR}_{\mathrm{max}}}\right]^2\right\}^{1/2}, \tag{16}$$

where $\mathrm{SNR}_{\mathrm{min}}$ and $\mathrm{SNR}_{\mathrm{max}}$ are signal-to-noise ratio (SNR) for P_{min} and P_{max}, respectively. Systematic errors in estimated P_{Ray} are given as

$$\left(\frac{\delta P_{\mathrm{Ray}}(r)}{P_{\mathrm{Ray}}(r)}\right)_{\mathrm{sys}} = \frac{2\beta_1(r)\Delta X_1^{\mathrm{min}}}{\beta_2(r)(1 - 2X_1^{\mathrm{min}})}. \tag{17}$$

Random errors in retrieved α_1 decrease as SNR increases, and the lower X_1^{min} reduces the errors [Fig. 4(a)]. For example, if $\mathrm{SNR}_{\mathrm{min}} > 1000$, the error in extinction retrieval is <9% at $X_1^{\mathrm{min}} = 0.37$, but the error is <2% at $X = 0.01$. Systematic errors in extinction retrieval drastically decrease as X_1^{min} decreases [Fig. 4(b)]. In our system, X_1^{min} is 0.37, and consequently $\Delta X_1^{\mathrm{min}}/X_1^{\mathrm{min}}$ must be sufficiently small (~1%). We use an analysis method to determine P_{max} and P_{min} (X_1^{min} and X_1^{max}) using all data taken in the periodical scan by fitting theoretical (sinusoidal) curves to the signals at each range (and reference signals). It is not difficult to achieve $\Delta X_1^{\mathrm{min}}/X_1^{\mathrm{min}} = 1\%$.

The use of a long interferometer raises another problem with angular dependence of the optical path difference of the interferometer [15]. If the angular distribution of the atmospheric

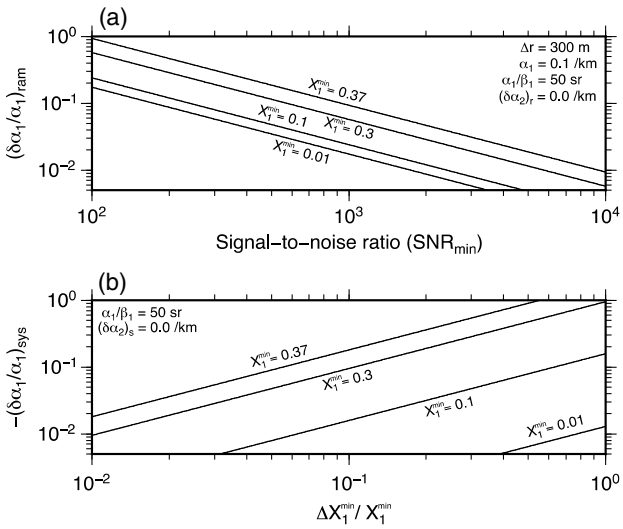

Fig. 4. (a) Random errors in retrieved α_1 for $\mathrm{SNR}_{\min}$. (b) Systematic errors in retrieved α_1 for $\Delta X_1^{\min}/X_1^{\min}$.

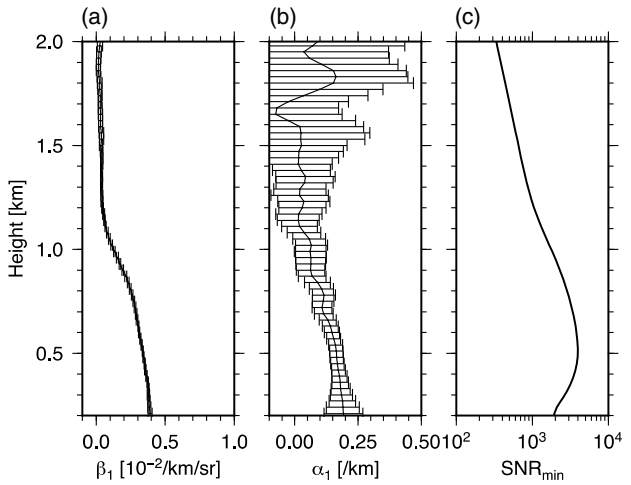

Fig. 6. (a) Backscattering coefficient, (b) extinction coefficient, and (c) signal-to-noise ratio derived from the MM-HSRL signals measured for 15 min from 11:40 a.m. (local time) on 17 February 2017 at Tsukuba, Japan. The error bars in (a) and (b) denote random errors.

scattering intensity varies with the height, $X_1^{\min}$ for the atmospheric scattering depends on the height and differs from $X_1^{\min}$, determined from the reference signals. To reduce the effect, the field-of-view (FOV) of the receiver telescope of our experimental MM-HSRL is limited to 0.1 mrad. With the narrow FOV, the geometrical form factor does not reach 1.0 up to high altitude (6000 m). The narrow FOV, however, also has advantages in reducing daytime background radiation and in reducing the dynamic range of the signals at the lower heights [16]. In our experimental system, we employ an additional telescope with a wide FOV (1 mrad) for evaluating the geometrical form factor of the MM-HSRL system and for measuring the depolarization ratio of the backscattering signals.

5. PRELIMINARY RESULTS

Figure 5 shows scanned X_1 data with the reference signals. The scanning range corresponds to one fringe (i.e., the laser mode spacing). The phase shift was corrected by fitting a curve every scan. Then the model curve was fitted (solid line in Fig. 5) with Eq. (11). Figure 6 shows backscattering and extinction coefficients measured during daytime. Scanned atmospheric scattering data were fitted in the same manner as the reference signals to obtain $P_{\mathrm{rat}}^{\min}$. Backscattering coefficient was calculated using $X_1^{\min}$ and $P_{\mathrm{rat}}^{\min}$ as Eq. (4). P_{ray} was derived by subtracting P_{bias} from $P_{\min}$, and, finally, the extinction coefficient was calculated. The geometric form factor in Eq. (7) was corrected with an elastic lidar having a larger FOV and measuring at the same period. Error bars in Fig. 6 were calculated with Eq. (12) for the backscattering coefficient and Eq. (14) for the extinction coefficient. The SNR used for the calculation is shown in Fig. 6(c). The errors in the extinction coefficient are large above the boundary layer, but the 15 min average time (i.e., 9000 shots) is sufficient for retrieving the extinction coefficient at lower aerosol layers where the SNR exceeds 1000. The random errors in the backscattering coefficient are very small compared to those in the extinction coefficient.

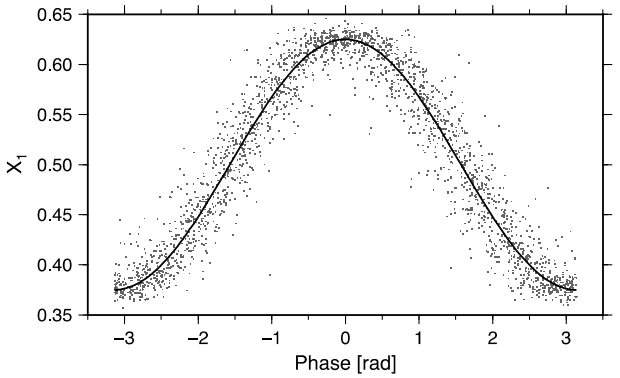

Fig. 5. Phase-corrected, scanned X_1 data for reference signals measured on 12 July 2016.

6. CONCLUSION

In this study, we described an algorithm for retrieving backscattering and extinction coefficients from HSRL measurement with a multimode laser and a scanning Mach–Zehnder interferometer. With the experiments reported in this paper, we confirmed that the MM-HSRL method is feasible. This study demonstrated daytime measurement of the aerosol extinction coefficient. We estimated the random errors for a Raman lidar with the same laser power and the same telescope size in nighttime using the same aerosol profile as in Fig. 6. The error for the MM-HSRL obtained in daytime measurement was comparable to the estimated nighttime Raman lidar measurement. The result showed that our target of this study (mentioned in the Introduction) was barely achieved. However, the experimental error in the extinction coefficient measurement with the current MM-HSRL was approximately 5 times larger than the theoretical error for the system. For this reason, we will continue improving the current system by replacing suspicious optical elements.

We are also studying possible improvement of the MM-HSRL system. The rejection rate for the Mie scattering is much less than that in single-mode HSRLs that utilize a filter with much wider spectral width than the single-mode lasers. The rejection rate will be improved by using multimode lasers with a narrower spectral width (longer pulse length). The difficulties of the MM-HSRL also arise from the use of a long interferometer. That results in the narrow FOV of the receiver system. Using a multimode laser with wider mode spacing (short cavity length) will reduce the length of the interferometer at the receiver, and that will allow wider receiver FOV. A technique similar to the field-widened Michelson interferometer [17] also may be applied to a Mach–Zehnder interferometer. With the technique, if a medium with a high refractive index is embedded in the long-arm side of the interferometer, the interferometer length can be reduced.

Funding. Japan Science and Technology Agency (JST); Japan International Cooperation Agency (JICA).

REFERENCES

1. G. G. Fiocco, G. Beneditti-Michelangeli, K. Maischberger, and E. Madonna, "Measurement of temperature and aerosol to molecule ratio in the troposphere by optical radar," Nature **229**, 78–79 (1971).
2. S. T. Shipley, D. H. Tracy, E. W. Eloranta, J. T. Trauger, J. T. Sroga, F. L. Roesler, and J. A. Weinman, "High spectral resolution lidar to measure optical scattering properties of atmospheric aerosols. 1: theory and instrumentation," Appl. Opt. **22**, 3716–3724 (1983).
3. H. Shimizu, S. A. Lee, and C. Y. She, "High spectral resolution lidar system with atomic blocking filters for measuring atmospheric parameters," Appl. Opt. **22**, 1373–1381 (1983).
4. P. Piironen and E. W. Eloranta, "Demonstration of a high-spectral-resolution lidar based on an iodine absorption filter," Opt. Lett. **19**, 234–236 (1994).
5. Z. Liu, I. Matsui, and N. Sugimoto, "High-spectral-resolution lidar using an iodine absorption filter for atmospheric measurements," Opt. Eng. **38**, 1661–1670 (1999).
6. J. W. Hair, C. A. Hostetler, A. L. Cook, D. B. Harper, R. A. Ferrare, T. L. Mack, W. Welch, L. R. Izquierdo, and F. E. Hovis, "Airborne high spectral resolution lidar for profiling aerosol optical properties," Appl. Opt. **47**, 6734–6752 (2008).
7. M. Esselborn, M. Wirth, A. Fix, B. Weinzierl, K. Rasp, M. Tesche, and A. Petzold, "Spatial distribution and optical properties of Saharan dust observed by airborne high spectral resolution lidar during SAMUM 2006," Tellus **61B**, 131–143 (2009).
8. D. Bruneau, J. Pelon, F. Blouzon, J. Spatazza, P. Genau, G. Buchholtz, N. Amarouche, A. Abchiche, and O. Aouji, "355-nm high spectral resolution airborne lidar LNG: system description and first results," Appl. Opt. **54**, 8776–8785 (2015).
9. A. J. Illingworth, H. W. Barker, A. Beljaars, M. Ceccaldi, H. Chepfer, N. Clerbaux, J. Cole, J. Delanoë, C. Domenech, D. P. Donovan, S. Fukuda, M. Hirakata, R. J. Hogan, A. Huenerbein, P. Kollias, T. Kubota, T. Nakajima, T. Y. Nakajima, T. Nishizawa, Y. Ohno, H. Okamoto, R. Oki, K. Sato, M. Satoh, M. W. Shephard, A. Velázquez-Blázquez, U. Wandinger, T. Wehr, and G.-J. van Zadelhoff, "The earthcare satellite: the next step forward in global measurements of clouds, aerosols, precipitation, and radiation," Bull. Am. Meteorol. Soc. **96**, 1311–1332 (2015).
10. S. P. Burton, R. A. Ferrare, C. A. Hostetler, J. W. Hair, R. R. Rogers, M. D. Obland, C. F. Butler, A. L. Cook, D. B. Harper, and K. D. Froyd, "Aerosol classification using airborne high spectral resolution lidar measurements—methodology and examples," Atmos. Meas. Tech. **5**, 73–98 (2012).
11. T. Nishizawa, N. Sugimoto, I. Matsui, A. Shimizu, B. Tatarov, and H. Okamoto, "Algorithm to retrieve aerosol optical properties from high-spectral-resolution lidar and polarization Mie-scattering lidar measurements," IEEE Trans. Geosci. Remote Sens. **46**, 4094–4103 (2008).
12. I. A. Razenkov, E. W. Eloranta, J. P. Hedrick, R. E. Holz, R. E. Kuehn, and J. P. Garcia, "A high-spectral resolution Lidar designed for unattended operation in the Arctic," in *21st International Laser Radar Conference* (International Corrdinating Group for Laser Atmospheric Studies, 2002).
13. D. Bruneau, F. Blouzon, J. Spatazza, F. Montmessin, J. Pelon, and B. Faure, "Direct-detection wind lidar operating with a multimode laser," Appl. Opt. **52**, 4941–4949 (2013).
14. P. Ristori, L. Otero, Y. Jin, N. Sugimoto, T. Nishizawa, and E. Quel, "Development of a high spectral resolution lidar using a multimode laser and a tunable interferometer," in *27th International Laser Radar Conference* (International Corrdinating Group for Laser Atmospheric Studies, 2015), paper PS A3.05-220.
15. Y. Jin, N. Sugimoto, T. Nishizawa, P. Ristori, and L. Otero, "A concept of multi-mode high spectral resolution lidar using Mach–Zehnder interferometer," in *27th International Laser Radar Conference* (International Corrdinating Group for Laser Atmospheric Studies, 2015), paper S2.06-286.
16. J. D. Spinhirne, "Micro pulse lidar," IEEE Trans. Geosci. Remote Sens. **31**, 48–55 (1993).
17. D. Liu, C. Hostetler, I. Miller, A. Cook, and J. W. Hair, "System analysis of a tilted field-widened Michelson interferometer for high spectral resolution lidar," Opt. Express **20**, 1406–1420 (2012).